Discrete & Continuous Models
& Applied Computational Science
ISSN 2658-7149 (online), 2658-4670 (print)

2023, 31 (2) 174–188
http://journals.rudn.ru/miph

Research article

UDC 519.624.2:531.8
PACS 62.20
DOI: 10.22363/2658-4670-2023-31-2-174-188
EDN: XEAYRS

Buckling in inelastic regime of a uniform console with symmetrical cross section: computer modeling using Maple 18

Viktor V. Chistyakov, Sergey M. Soloviev

Laboratory of Rare Earth Semiconductor Physics,
Physical-Technical Institute named after A.F. Ioffe of RAS,
26, Politekhnicheskaya St., Saint Petersburg, 194021, Russian Federation

(received: February 5, 2023; revised: May 7, 2023; accepted: June 26, 2023)

Abstract. The method of numerical integration of Euler problem of buckling of a homogeneous console with symmetrical cross section in regime of plastic deformation using Maple 18 is presented. The ordinary differential equation for a transversal coordinate y was deduced which takes into consideration higher geometrical momenta of cross section area. As an argument in the equation a dimensionless console slope $p = \operatorname{tg}\theta$ is used which is linked in mutually unique manner with all other linear displacements. Real strain-stress diagram of metals (steel, titan) and PTFE polymers were modelled via the Maple nonlinear regression with cubic polynomial to provide a conditional yield point (t,σ_f). The console parameters (free length l_0, m, cross section area S and minimal gyration moment J_x) were chosen so that a critical buckling forces F_{cr} corresponded to the stresses σ close to the yield strength σ_f. To find the key dependence of the final slope p_f vs load F needed for the shape determination the equality for restored console length was applied. The dependences $p_f(F)$ and shapes $y(z)$, z being a longitudinal coordinate, were determined within these three approaches: plastic regime with cubic strain-stress diagram, tangent modulus E_{tang} approximations and Hook's law. It was found that critical buckling load F_{cr} in plastic range nearly two times less of that for an ideal Hook's law. A quasi-identity of calculated console shapes was found for the same final slope p_f within the three approaches especially for the metals.

Key words and phrases: Euler problem, plane cross-sections hypothesis, buckling, console, plastic deformation, strain-stress diagram, conditional yield point, critical buckling load, Maple programming, nonlinear estimation, Al/PTFE, steel

1. Introduction

The problem of stability loss in a beam under longitudinal load (buckling) in the range of inelastic strains is actual and important from many points of view such as sports (pole vaulting), civil engineering (bridges, truss constructions), aeronautics, robotics and elsewhere the requirements of a small weight and large strength are imposed on structural elements been designed [1]. Fatigue of materials, lowering the proportionality and elasticity limit due to the Bauschinger effect in periodically tensile and compressed elements, hysteresis etc. — all that results in falling of initially secure loads time into the zone of serious risk of buckling. Therefore, beginning from the pioneering work of F.R. Shanley [2] considered so called tangent and reduced moduli approaches [ibid], Euler's problem in inelastic range attracts more and more researchers — from engineers dealing with material strength to pure mechanicians and mathematicians dealing with bifurcations, nonlinear phenomena etc.

Of course, modern models of buckling are 2- or even 3-dimensional and they take into account not only bending shift component but a shear one too. To take all this into account the finite-element modeling (FEM) is widely used and it is implemented in the commercial software package ABAQUS (see e.g. [3–5]) and similar software. Many features and peculiarities both in thick so called Timoshenko beams [6] and in sandwich/fiber-composite/lattice/C-columns (see [7–9]) etc. are explained well in these multidimensional models.

The problem is studied in university courses of material sciences within a *plane cross-sections hypothesis* which leads to simple one-dimensional (1D) Euler ordinary differential equation (ODE) of the II-nd order. However, the attention is paid mainly to moment of arising of the phenomenon itself and its possible shapes for various ways of a beam fixation. Unfortunately, the linearized Euler ODE coupled with boundary condition (BC) on the beam ends looks like a classical eigenvalue problem with unstable higher modes corresponding to higher eigenvalues too. This ODE is similar to the Schröedinger equation for 1D particle in a potential well with infinitely high walls. This similarity misleads the students to the wrong conclusion that the non-zero solution of the ODE exists only for a set of "resonant" axial loads F_n, $n = 1, 2, ...$ just like in the aforementioned case of the well. And it is not clear whether for "non-resonant" forces from inside the intervals the ODE has purely compressive solution without any buckling or else power-like formula or something else. Or, may be, it shoots at some finite value at once just as the axial force F reaches some critical value as we have seen from our own experience, compressing by the hands a steel ruler? In what way the non-linear and inelastic properties with yield point on strain-stress diagram of real materials influence the critical buckling load $F_{\rm cr}$ and the shape of column buckled?

This kind of questions inevitably arises by analytically thinking students which can't find the answers in many available textbooks where only simplified explanation of the phenomenon is presented. One of the reasons why it takes place is traditionally pure mathematical means to describe the buckling process not expressing in standard algebraic functions. Nowadays, at the time of rapid development of mathematical software, more and more new opportunities to study the buckling phenomenon both with practical, scientific and educational purposes are opening up.

As for the Maple itself it is permanently improving software package with simple programming language with commands close to English ones supplied with comprehensive parameters and easily read option Help. The undeniable advantage of the package in addition to the extremely broad coverage of the sciences from Bayesian statistics to Feynman diagram calculations is an extremely high computational accuracy due to so-called "long Arithmetics" (Matlab soft uses Maple calculations) and opportunity to choose an alternative computational method and compare the results to improve their reliability. All above makes this package most reliable means of numerical modeling compared to those packages where the control of the calculation process is reduced only to the choice of the "mouse" option from the menu.

The work is devoted to numerical modeling of the buckling phenomenon of uniform beam. The main purpose of this work is to present readers relatively simple and effective calculation algorithm and its realization with the Maple 2018 relying on which it is possible to learn in what way inelastic and plastic properties of the material in question influence the basic parameters of buckling. The versatile skills gained from this activity may be then applied in up to date theories and experiments in study of buckling of real constructive elements say within aforementioned FEM and others.

The application of the Maple not only solves many technical difficulties of mathematical nature but with the algorithm itself and with consequence of computational procedures it gives students better comprehension of the mechanism and nature of the phenomenon of buckling. Moreover, as part of university lessons and practices this kind of investigations may be joined in one collective interdisciplinary research project which results may be discussed, analyzed and then presented at student conference/contest.

2. Equation

We neglect in the paper the shear effects and stay within the classical Euler's 1D-model of buckling but with the axial compressive loads resulting in plastic deformations in the material.

Nevertheless, the fundamental properties of the phenomenon are described adequately both from qualitative and quantitative points of view in the frames. And the results of modelling with the use of software package Maple 18 fit well compressive tests for various real materials with non-linear strain-stress diagram.

We regard for simplicity the vertical column AB of free length l and uniform cross-section (S) symmetrical with respect to the axis x of minimal gyration. The column is made of isotropic material with a typical for metals and polymers strain-stress diagram with conditional yield point (see later). The lower end A of the column is pinned hardly while the upper one B been exposed to the axial compressive load F, N (figure 1). This vertical force provides normal stresses σ_n beyond the elastic range on the diagram, and even greater than yield strength σ_f above.

The choice of the pinned console solves problems with ambiguity of the bonds between the slope and the axis displacements. So, the transversal shift y of the center of the z cross-section and its vertical displacement Δz are uniquely related to the current inclination $p = dy/dz$ of the console axis (figure 2).

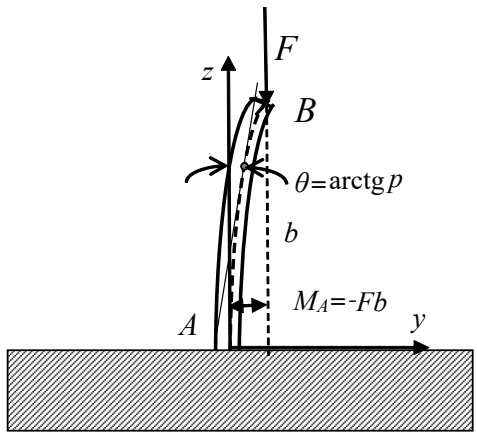

Figure 1. The uniform beam with pinned lower end A and loaded with F on the upper B

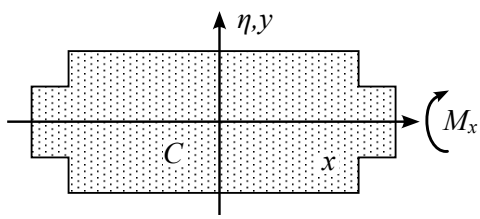

Figure 2. Symmetrical cross-section with zero odd momenta

Let's write down the fundamental relation between bending torque $M_x(z)$ and curvature radius ρ (z) in the same section (z). First, within plane-section hypothesis we represent the normal strain in the layer with the local coordinate η as $\varepsilon_\eta = \varepsilon_{ax} + \eta/\rho$ where ε_{ax} is a compressive strain of the axis crossing the section z in the center C.

Then regarding strain-stress diagram as obeying cubic law with respect to the access value we have

$$\sigma(\varepsilon) = \sigma(\varepsilon_{ax}) + \frac{d\sigma(\varepsilon_{ax})}{d\varepsilon}\frac{\eta}{\rho} + \frac{1}{2!}\frac{d^2\sigma(\varepsilon_{ax})}{d\varepsilon^2}\left(\frac{\eta}{\rho}\right)^2 + \frac{1}{3!}\frac{d^3\sigma(\varepsilon_{ax})}{d\varepsilon^3}\left(\frac{\eta}{\rho}\right)^3.$$

Substituting this expression into the formula for the bending moment and taking into account the symmetry of the cross-section, we get

$$M_x(z) = \iint \sigma_z \eta dS = \frac{d\sigma(\varepsilon_{ax})}{d\varepsilon}\frac{J_x^{(II)}}{\rho} + \frac{1}{3!}\frac{d^3\sigma(\varepsilon_{ax})}{d\varepsilon^3}\frac{J_x^{(IV)}}{\rho^3},$$

with $J_x^{(II)}$ and $J_x^{(IV)}$ being the 2-nd and 4-th momenta of inertia of the cross-section area. The 3-rd one drops due to the cross-section symmetry and we may generalize the concept of a cross-section symmetry in this way, i.e. $J_x^{(III)} = 0$.

Given that $1/\rho$ equals $y''_{zz}/(1+y'^2_z)^{3/2}$, we get the left-hand side and writing down the right-hand side the equation which determines the shape of the column buckled

$$\frac{d\sigma(\varepsilon_{ax})}{d\varepsilon}\frac{J_x^{(II)}y''_{zz}}{(1+y'^2_z)^{\frac{3}{2}}}+\frac{1}{6}\frac{d^3\sigma(\varepsilon_{ax})}{d\varepsilon^3}\frac{J_x^{(IV)}(y''_{zz})^3}{(1+y'^2_z)^{\frac{9}{2}}}=-(Fy+M_A), \tag{1}$$

with $M_A=-Fb$ being a torque on hard seal A (figure 1) and the value of b as a transversal shift of the upper end B.

This equation is nonlinear on the senior second derivative but due to its autonomy, it can be lowered in its order and then solved within the framework of perturbative approach under the assumption that the second term with $J_x^{(IV)}$ is much smaller than the first one. Thus, making the substitute $v=y-b$ we get the equation with boundary condition

$$\begin{cases}\dfrac{J_x^{(II)}v''_{zz}}{(1+v'^2_z)^{\frac{3}{2}}}\left(\dfrac{d\sigma(\varepsilon_{ax})}{d\varepsilon}\right)+\dfrac{1}{6}\left(\dfrac{d^3\sigma(\varepsilon_{ax})}{d\varepsilon^3}\right)\dfrac{J_x^{(IV)}v''^3_{zz}}{(1+v'^2_z)^{\frac{9}{2}}}=-Fv,\\ v(0)=-b,\quad v(z_B)=0,\quad v'_z(0)=0.\end{cases}$$

After substitution $v'=p$ and assigning the p as an argument we get $v''_{zz}=p\cdot(dp)/(dv)$ and

$$\begin{cases}\dfrac{J_x^{(II)}p\frac{dp}{dv}}{(1+p^2)^{\frac{3}{2}}}\left(\dfrac{d\sigma(\varepsilon_{ax})}{d\varepsilon}\right)+\dfrac{1}{6}\left(\dfrac{d^3\sigma(\varepsilon_{ax})}{d\varepsilon^3}\right)\dfrac{J_x^{(IV)}(p\frac{dp}{dv})^3}{(1+p^2)^{\frac{9}{2}}}=-Fv,\\ v(0)=-b,\quad v(p_f)=0,\end{cases}$$

where p_f is a final slope at the end B.

After simple transformation we receive

$$\begin{cases}\dfrac{J_x^{(II)}dp^2}{(1+p^2)^{\frac{3}{2}}}\dfrac{d\sigma(\varepsilon_{ax})}{d\varepsilon}+\dfrac{1}{6}\dfrac{d^3\sigma(\varepsilon_{ax})}{d\varepsilon^3}\dfrac{J_x^{(IV)}v^2dp^2}{(1+p^2)^{\frac{9}{2}}(\frac{dv^2}{dp^2})^2}=-Fdv^2,\\ v^2(0)=b^2,\quad v(p_f^2)=0,\end{cases}\quad\Leftrightarrow$$

$$\Leftrightarrow\left|\begin{matrix}v^2\equiv w\\ p^2\equiv s\end{matrix}\right|\begin{cases}\dfrac{dw}{ds}=-\dfrac{J_x^{(II)}}{F(1+s)^{\frac{3}{2}}}\dfrac{d\sigma(\varepsilon_{ax})}{d\varepsilon}-\dfrac{1}{6}\dfrac{d^3\sigma(\varepsilon_{ax})}{d\varepsilon^3}\dfrac{J_x^{(IV)}w}{F(1+s)^{\frac{9}{2}}(\frac{dw}{ds})^2},\\ w(0)=b^2,\quad w(p_f^2)=0.\end{cases} \tag{2}$$

In this equation the derivatives $(d\sigma(\varepsilon_{ax}))/(d\varepsilon)$ and $(d^3\sigma(\varepsilon_{ax}))/(d\varepsilon^3)$ depend on $p^2=s$ because both the strain ε_{ax} of the axis and the normal stress σ_{ax} at certain place caused by it depend the slope p as

$$\sigma_{ax}(p)=\frac{F\cos\theta}{S}=\frac{F}{S(1+p^2)^{\frac{1}{2}}}=\frac{F}{S(1+s)^{\frac{1}{2}}}. \tag{3}$$

Also, the final slope p_f is unknown and it should be found from some condition (see later). To solve (2) we should build and use a model strain-stress diagram both in direct and inverse type.

3. Modelling strain-stress diagram

We considered the diagrams which contain a) initial proportionality stage $\sigma(\varepsilon) = E\varepsilon$, the E being Young's modulus, b) the yield stage containing *conditional yield point* (σ_f, t), i.e. an inflection point with $(d^2\sigma(t))/(d\varepsilon^2) = 0$, c) and final *densification* stage with $(d^2\sigma(\varepsilon))/(d\varepsilon^2) > 0$.

The cubic formula meeting all the requirements above is as follows

$$\sigma(\varepsilon) = E\varepsilon - \frac{3E\mu}{2}\varepsilon^2 + \frac{E\mu}{2t}\varepsilon^2, \quad \mu = \frac{Et - \sigma_f}{Et^2}, \tag{4}$$

and it has the derivatives

$$\frac{d\sigma(\varepsilon)}{d\varepsilon} = E - 3E\mu\varepsilon + \frac{3E\mu}{2t}\varepsilon^2, \quad \frac{d^3\sigma(\varepsilon)}{d\varepsilon^3} = \frac{3E\mu}{t}. \tag{5}$$

(The parameter μ turns to zero at ideal linear diagram otherwise it describes in what extent the diagram is nonlinear. Namely, the greater μ the more non-linear $\sigma(\varepsilon)$-dependence and it manifests itself at smaller strains ε.)

For the equation (3) it corresponds to reverse approximate formula

$$\varepsilon(\sigma) = \frac{\sigma}{E} + \frac{3\mu\sigma^2}{2E^2} + \frac{\mu(9\mu t - 1)\sigma^3}{2E^3 t} \tag{6}$$

which gives identity with accuracy of $O(\varepsilon^4)$ when the stress value (3) is substituted into it.

Application of (4) for regression by Maple 2018 option "*Fit*" on experimental data received at students' practicum for low carbon steel compression test gives good match on the level of adjusted $R^2 = 0.999733$ of the data with the curve (3) (figure 3). An estimated Young's modulus E lies in confidence (95%) interval (165; 175) GPa a little less of the handbook values of 180 ... 220 GPa. This is surely due to fatigue of the material as a result of numerous tests fulfilled by many generations of students in the workshop on material science at Yaroslavl branch of Moscow Institute of Transport Engineers.

The reversed formula (6) also fits well the data within yield stage though it doesn't contain a densification stage. Up to the beginning of the densification stage due to (3), the curves actually merge into a single line with discrepancies being of order of the residuals of estimation. Also, we see good quasi-linearity of the data in range of εs from about 0.007 to ~ 0.017 where the conditional yield point ($t = 0.0134$) is localized. This quasi-linearity justifies the use of the tangent modulus method in solving the Euler equation for buckled beam.

Not only for the steel but for other metals such as titan and wolfram the simple cubic formulas (4) and (6) fit well the experimental data. For the fluor polymers they hold too. Thus, for Al/PTFE (aluminum/polytetrafluoroethylene) the experimental data [10] fit well (4) (figure 4). Moreover, we see that

in the wide enough middle part of the diagram points fit well on a straight line corresponding to the tangent modulus Et of about 50 MPa. Although the interpolating line does not emphasize this fact.

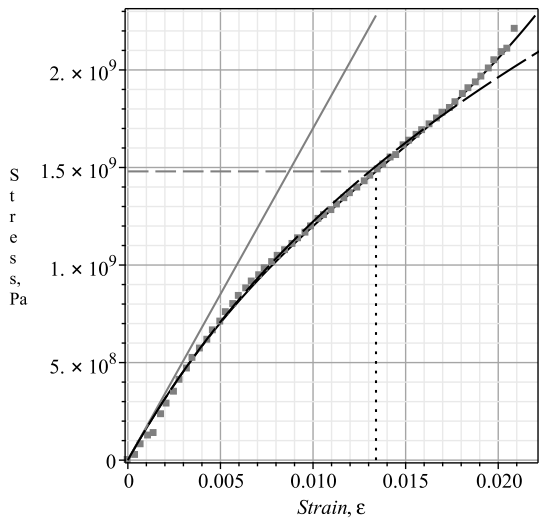

Figure 3. Cubic model direct (4) (grey solid) and reverse (6) (black long dash) diagrams built on experimental data (black diamonds) for low carbon steel. Hook's law (solid thin grey), yield strain $t = 0.0134$ (black dot), yield stress $\sigma_f = 1.48 \cdot 10^9$ Pa (grey dash)

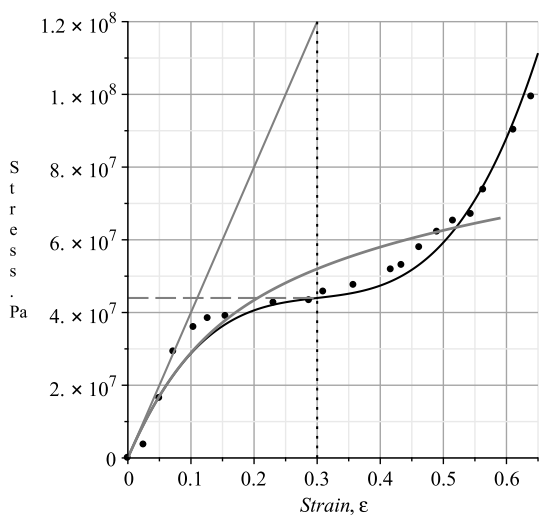

Figure 4. Al/PTFE strain-stress diagram: experiment [10] (solid circle); cubic model $\sigma(\varepsilon)$ (4) with the parameters $E = 400$ MPa, $\sigma_f = 44$ MPa, $t = 0.3$, $E_{\text{tang}} = 55.8$ MPa (solid black), Hook's law (solid thin grey), reversed diagram $\varepsilon(\sigma)$ (solid thick grey), yield strain $t = 0.3$ (black dot), yield strength (grey long dash)

All examples above confirm the effectiveness of a simple cubic formula for adequate describing the diagrams of many plastic materials, both metals and polymer composites, increasingly used in mechanical engineering, aeronautics and robotics.

4. Solving the equation

To write down the equation describing the buckling in inelastic regime we should substitute (6) in the formula (5) for the first derivative and limit the resulting expression to the first four members

$$\frac{d\sigma}{d\varepsilon} = E - 3\mu\sigma + \left(\frac{3\mu}{2Et} - \frac{9\mu^2}{2E}\right)\sigma^2 + \left(\frac{6\mu^2}{E^2t} - \frac{27}{2E^2}\right)\sigma^3. \tag{7}$$

Substituting the expression (3) for axial stress in (7) and then in (2) we receive the equation defining the dependence $w = v^2 \cdot vs \cdot s = p^2$.

$$\frac{dw}{ds} = -\frac{J_x^{(II)}}{F(1+s)^{\frac{3}{2}}} + \frac{3J_x^{(II)}\mu}{S(1+s)^2} - \frac{J_x^{(II)}\left(\frac{3\mu}{2Et} - \frac{9\mu^2}{2E}\right)}{S^2(1+s)^{\frac{5}{2}}}F - \\ - \frac{J_x^{(II)}\left(\frac{6\mu^2}{E^2t} - \frac{27}{2E^2}\right)}{S^3(1+s)^3}F^2 - \frac{\mu E}{2t}\frac{J_x^{(IV)}w}{F(1+s)^{\frac{9}{2}}\left(\frac{dw}{ds}\right)^2}. \tag{8}$$

Expressing the $w = w_0 + \delta w$ as a sum of the w_0 satisfying the equation (8) with $J_x^{(IV)} = 0$ and boundary conditions in (2), and a small additive δw fitting zero boundary conditions at upper end B, we find formulas for the w_0 and δw:

$$w_0(s) = \frac{2J_x^{(II)}}{F(1+s)^{\frac{3}{2}}} - \frac{3J_x^{(II)}\mu}{S(1+s)^2} + \frac{2J_x^{(II)}\left(\frac{3\mu}{2Et} - \frac{9\mu^2}{2E}\right)}{3S^2(1+s)^{\frac{5}{2}}}F + \\ + \frac{J_x^{(II)}\left(\frac{6\mu^2}{E^2t} - \frac{27}{2E^2}\right)}{2S^3(1+s)^3}F^2 - b^2, \tag{9}$$

$$\delta w(s) = \frac{\mu E J_x^{(IV)}}{2Ft}\int_s^{p_f^2} \frac{w_0(s')ds'}{(1+s')^{\frac{9}{2}}\left(\frac{dw_0}{ds'}\right)^2}. \tag{9'}$$

From (8) a clear relationship between the transversal displacement b of the upper end B of the console and its final slope p_f follows

$$b = \left\{ \frac{2J_x^{(II)}}{F(1+p_f^2)^{1/2}} - \frac{3J_x^{(II)}}{S(1+p_f^2)^2} + \frac{2J_x^{(II)}\left(\frac{3\mu}{2Et} - \frac{9\mu^2}{2E}\right)}{3S^2(1+p_f^2)^{5/2}}F + \right.$$

$$+\frac{J_x^{(II)}\left(\frac{6\mu^2}{E^2t}-\frac{27}{2E^2}\right)}{2S^3(1+p_f^2)^3}F^2+\frac{\mu E J_x^{(IV)}}{2Ft}\int\limits_s^{p_f^2}\frac{w_0(s')ds'}{(1+s')^{\frac{9}{2}}\left(\frac{dw_0}{ds'}\right)^2}\Bigg\}^{1/2}. \quad (10)$$

Further calculations (see later) show that for real materials and standard cross sections (I,L-beam, channel, square, circle, etc.) the addition (9′) is at least 4 orders less than basic function (8). Thus, for a PTFE Teflon channel with a length of $l_0 = 0.75$ m and an area 64 times the area of channel No. 10 at a final slope of 0.5, the additive δw was in maximum less than 0.01% of the basic function $w_0(s = p^2)$. And since they are added geometrically to form $v(p) = y(p) - b$, the contribution will be completely invisible (figure 5). So, we may easily neglect the integral amendment in (10).

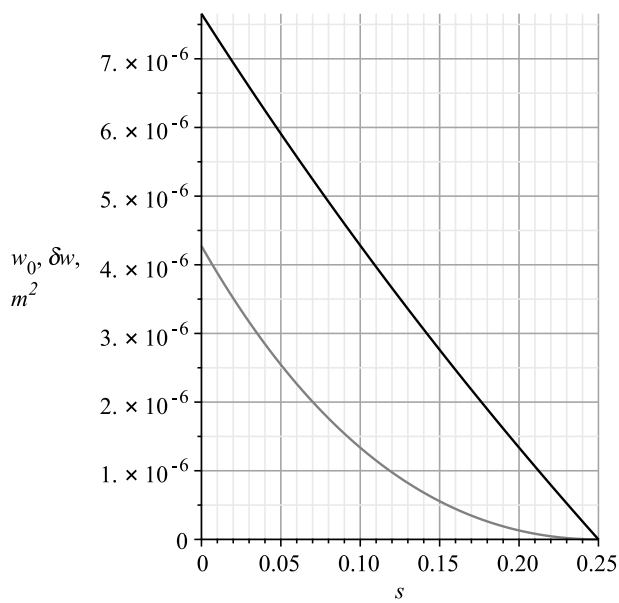

Figure 5. First order function $10^{-4}w_0(s = p^2)$ (black) (9) and additive δw (grey) (9′) due to 4-th moment of inertia $J_x^{(IV)}$ for I-beam made of Teflon (PTFE), 0.75 m, 0.077 m^2, $J_x^{(II)} = 0.000065124$ m^4

5. Determining the final slope vs load dependence

Analyzing the expressions (8)–(10) it is easily seen that correct solution of ODE may be received only for known dependence of the load F on the final slope p_f. To find it we are to compile so called characteristic equation on restored length of the console.

So, we have a transversal axis shifted coordinate $v_0(p) = y(p) - b = -\sqrt{w_0(p^2)}$.

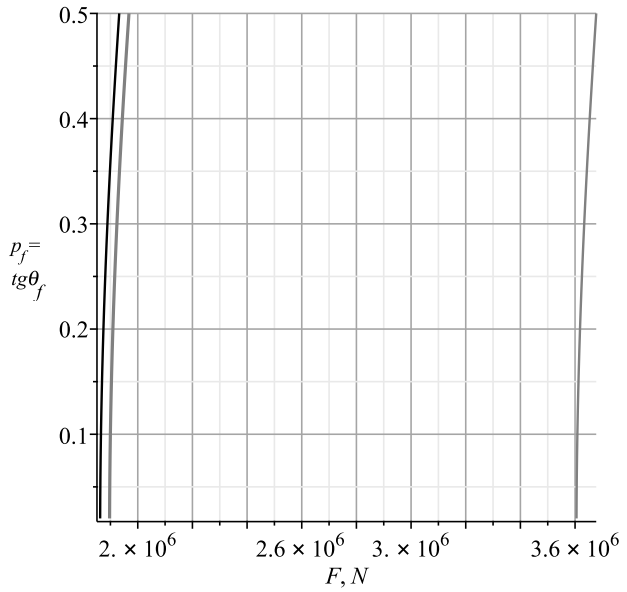

Figure 6. The $p_f(F)$ dependences for Al/PTFE I-console with $l_0 = 0.5$ m, $S = 0.077$ m^2, $J_x^{(II)} = 0.000065124$ m^4 within the three approaches: stress due (4) (black), tangent modulus (thick grey) and Hook's law (grey thin)

The longitudinal coordinate z may be found as $z(p) = \int_0^p \frac{dv_0(p')}{p'}$ and elementary length of the axis as

$$dl(p) = \frac{dv_0(p)}{p}\sqrt{1+p^2} = -\frac{d\sqrt{w_0}}{ds}\cdot\frac{dw_0}{ds}\cdot\frac{ds}{dp}\cdot\frac{\sqrt{1+p^2}}{p} = -\frac{dw_0}{ds}\frac{\sqrt{1+p^2}}{\sqrt{w_0}}.$$

Being restored after the load is removed, this value becomes

$$dl_{\text{res}}(p) = \frac{dl(p)}{1-\varepsilon(p)} \approx \frac{dw_0}{dp^2}\cdot\frac{\sqrt{1+p^2}}{\sqrt{w_0}}\left(1+\varepsilon(p)+\varepsilon^2(p)+\varepsilon^3(p)\right),$$

where the strain $\varepsilon(p)$ taken positive, of the console axis element marked p is received by substitution of the stress (3) in the reverse strain-stress diagram (6). By integrating by p and equating the result with the free length of the console l_0, we obtain the function $p_f(F)$ specified implicitly:

$$-\int_0^{p_f}\frac{dw_0}{dp^2}\cdot\frac{\sqrt{1+p^2}}{\sqrt{w_0}}\left(1+\varepsilon(p)+\varepsilon^2(p)+\varepsilon^3(p)\right)dp = L(F,p_f) = l_0. \quad (11)$$

This key equation has non-empty solution if and only if the value of load F exceeds some critical buckling force F_{cr}, The Maple package has successful

option *implicitplot* which builds precisely the graphs of implicitly specified functions.

To compare the results obtained at different approximations, dependencies $p_f(F)$ were also calculated for an ideal material with the same Young's modulus, as well as in the approximation of a tangent module when the first derivative in (7) was limited by the first two terms $\frac{d\sigma}{d\varepsilon}(\sigma) = E - 3\mu\sigma$.

Due to the availability of a quasilinear middle yield stage on the diagrams (figures 4) for Al/PTFE (aluminum/polytetrafluoroethylene) [ibid], the results for the cubic formula (4) obtained within the tangent modulus approach were very close, but hugely differing from the results within Hook's law (figure 5).

It is worth mentioning that the extremely large loads were chosen exclusively to reach the stresses close to yield strength σ_f. For the same reason, the geometric parameters of the console were chosen, so that its flexibility λ varied from ~ 5 to ~ 20.

So, we see that regime of plastic deformations diminishes cardinally the classical critical load F_{cr} predicted by Hook's law approach studied in most universities. Especially it takes place for the materials with low yield strength such as Teflon, polymers in general and composites based on them.

Also, we see that relatively simple tangent modulus approach gives the results extremely close to those received by modeling strain-stress diagram by cubic formula (4) with conditional yield point.

The cross-section symmetry in generalized meaning, i.e., $J_x^{(III)} = 0$ simplifies significantly the calculation due to the absence of a next-in-rank additive. And as for this for the 4-th gyration moment it occurs quite negligible so we may limit ourselves to only the terms containing the second moment of the cross-section. As for widely used non-symmetrical cross-sections such as L-beam the 3-rd moment doesn't equal exactly to zero but very close to it due to the area quasi-anti-symmetry. Thus, the method developed may be implemented for wide class of constructive profiles.

6. Buckling shape

The shape of the buckled console is easily calculated parametrically from the above formulas for the longitudinal $z(p)$ and transversal $y(p)$ coordinates. The shape was calculated in all three approximations: the plastic deformations of the axis due to a model cubic diagram with a conditional yield strength, in the approximation of the tangent modulus, and for Hook's law. The load F for each case was taken to provide the same final slope $p_f = 0.5$ (figures 7, 8).

We see that the shapes are extremely close to each other though the compressed lengths differ significantly especially for ideal Hook's case with the load almost 2 times greater of those for the rest two approaches. As for the case of the low carbon steel with much greater Young's modulus the identity of the shapes was really ideal (figures 8) for different beam lengths. Due to approximate proportionality of the loads providing the same final slope within different approaches one may suggest not to solve the unwieldy case of cubic diagram (4) but to use a simple Hookean case with the subsequent recalculation of forces.

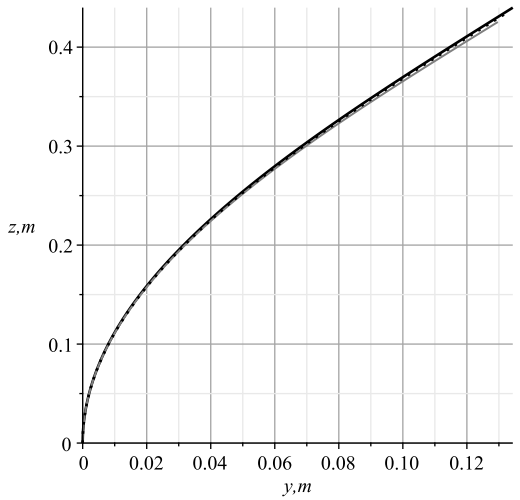

Figure 7. Quasi-identity of the shape of the Al/PTFE I-console, $l_0 = 0.5$ m. 0.077 m^2, $J_x^{(II)} = 0.000065124$ m^4 buckled under the loads $F(p_f = 0.5)$ within the three approaches: plastic strain (4) under $F = 1.932 \cdot 10^6 N$ (black solid), tangent modulus with $F = 1.97 \cdot 10^6 N$ (black dot) and Hook's law with $F = 3.68 \cdot 10^6 N$ (grey)

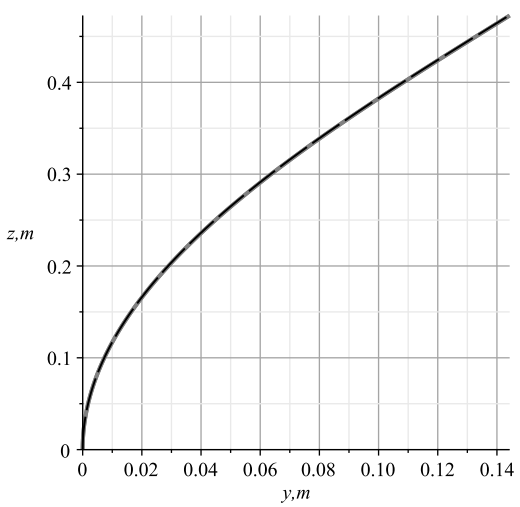

Figure 8. Really complete shape identity for the steel I-console No 10, $l_0 = 0.5$ m under loads resulting in equal p_f of 0.5 due to ideal Hook's (black long dash) and cubic (solid grey) strain-stress diagram

7. Conclusion

So, we prove that the suggested numerical method of Euler problem solution within a plane section hypothesis using the Maple software is quite effective and implementable in the range of plastic strains. The software is versatile

useful for solving many related sub-problems such as bringing together similar terms, expansion expression into a series, curve fitting, nonlinear estimation of parameters from experimental data, plotting an implicitly specified function, 3D-plots, etc. The algebraic type of the functions involved which is provided by a lucky choice of integration variable facilitates the computational process and gives a gain in speed compared to analogous use of transcendental and moreover special functions. Therefore, the method may be further generalized on more complicate case of piecewise uniform beam.

Solving this kind problems, when any even minor invisible error can mislead student to qualitatively wrong results and conclusions, disciplines him and eventually makes him a specialist in mathematical modeling in a wide range of sciences. The specialist who is critical of "ready-made solutions" in the form of convenient commercial software products which may solve well one class of problems and occur useless and distractive for another one.

References

[1] T. H. G. Megson, "Columns," in *Aircraft Structures for Engineering Students*, 6th. Elsevier Ltd., 2022, pp. 253–324.

[2] F. R. Shanley, "Inealstic Column Theory," *Journal of Aeronautical Sciences*, vol. 14, no. 5, pp. 261–280, 1947.

[3] A. Afroz and T. Fukui, "Numerical Analysis II: Branch Switching," in *Bifurcation and Buckling Structures*, 1st. CRC Press, 2021, p. 12.

[4] N. Shuang, J. R. Kim, and F. F. Rasmussen, "Local-Global Interaction Buckling of Stainless Steel I-Beams. II: Numerical Study and Design," *Journal of Structural Engineering*, vol. 141, no. 8, p. 04 014 195, 2014. DOI: 10.1061/(ASCE)ST.1943-541X.0001131.

[5] F. Shenggang, D. Daoyang, Z. Ting, *et al.*, "Experimental Study on Stainless Steel C-columns with Local-Global Interaction Buckling," *Journal of Constructional Steel Research*, vol. 198, no. 2, p. 107 516, 2022. DOI: 10.1016/j.jcsr.2022.107516.

[6] S. P. Timoshenko and J. M. Gere, *Theory of Elastic Stability*. NewYork, USA: McGraw-Hill, 1961.

[7] K. L. Nielsen and J. W. Hutchinson, "Plastic Buckling of Columns at the Micron Scale," *International Journal of Solids and Structures*, vol. 257, no. 5, p. 111 558, 2022. DOI: 10.1016/j.ijsolstr.2022.111558.

[8] A. Bedford and K. M. Liechti, "Buckling of Columns," in *Mechanics of Materials*, Springer, Cham., 2020. DOI: 10.1007/978-3-030-22082-2_10.

[9] Z. P. Bazant, "Shear buckling of sandwich, fiber-composite and lattice columns, bearings and helical springs: paradox resolved," *ASME Journal of Applied Mechanics*, vol. 70, pp. 75–83, 2003. DOI: 10.1115/1.1509486.

[10] C. Chuang, G. Zihan, and T. Enling, "Determination of Elastic Modulus, Stress Relaxation Time and Thermal Softening Index in ZWT Constitutive Model for Reinforced Al/PTFE," *Polymers*, vol. 15, p. 702, 2023. DOI: 10.3390/polym15030702.

For citation:

V. V. Chistyakov, S. M. Soloviev, Buckling in inelastic regime of a uniform console with symmetrical cross section: computer modeling using Maple 18, Discrete and Continuous Models and Applied Computational Science 31 (2) (2023) 174–188. DOI: 10.22363/2658-4670-2023-31-2-174-188.

Information about the authors:

Chistyakov, Viktor Vladimirovich (Russian Federation) — Candidate of Sciences in Physics and Mathematics, Senior Researcher of Laboratory of Physics of Rare Earth Semiconductors of Ioffe Physical-Technical Institute of the Russian Academy of Sciences (e-mail: `v.chistyakov@mail.ioffe.ru`, phone: +7(981) 815-74-95, ORCID: https://orcid.org/0000-0003-4574-0857, ResearcherID: F-9868-2016, Scopus Author ID: 44461256400)

Soloviev, Sergey Mikhailovich — Candidate of Sciences in Physics and Mathematics, Leading Researcher (Head of Laboratory) of Laboratory of Physics of Rare Earth Semiconductors of Ioffe Physical-Technical Institute of the Russian Academy of Sciences (e-mail: `serge.soloviev@mail.ioffe.ru`, phone: +7 (921) 439-62-13, ORCID: https://orcid.org/0000-0002-9019-7382, ResearcherID: D-5128-2015, Scopus Author ID: 7101661580)

УДК 519.624.2:531.8
PACS 62.20
DOI: 10.22363/2658-4670-2023-31-2-174-188
EDN: XEAYRS

Продольный изгиб однородной консоли с симметричным сечением в режиме пластических деформаций: численное моделирование посредством Maple 18

В. В. Чистяков, С. М. Соловьёв

Лаборатория физики редкоземельных полупроводников,
Физико-технический институт им. А. Ф. Иоффе РАН,
Политехническая ул., д. 26, Санкт-Петербург, 194021, Россия

Аннотация. Представлен способ численного моделирования посредством Maple 2018 продольного изгиба однородной консоли с симметричным сечением в режиме пластических деформаций. Получено обыкновенное дифференциальное уравнение для поперечной координаты, учитывающее высшие моменты инерции сечения. В качестве аргумента в нём служил уникальный для каждого места безразмерный наклон консоли $p = \tan\theta$, взаимно однозначно связанный со всеми перемещениями. Диаграммы сжатия реальных материалов (сталь, титан, тефлон, алюминий-тефлон) моделировались в Maple при помощи нелинейной регрессии на экспериментальных и литературных данных с использованием полинома 3-го порядка, обеспечивающего условный предел текучести (t,σ_f). Параметры консоли (длина l_0, площадь сечения S и минимальный момент инерции J_x) подбирались так, чтобы изгибающая сила обеспечивала напряжение вблизи предела текучести σ_f. Для нахождения ключевой зависимости углового наклона свободного конца p_f от закритической нагрузки $F > F_{\rm cr}$, что необходимо для определения формы прогиба, использовалось равенство проинтегрированной восстановленной элементарной длины её свободному значению l_0. Зависимости $p_f(F)$ и $y(z)$, z — продольная координата, рассчитывались в рамках следующих трёх подходов: пластический характер деформаций согласно полиномиальной $(n = 3)$ диаграмме, приближение касательного модуля $E_{\rm tang}$ и приближение идеальной выполнимости закона Гука. Обнаружено, что в реальном случае пластических деформаций критическая нагрузка $F_{\rm cr}$ почти вдвое меньше, чем в идеальном случае. При этом наблюдается почти идентичность формы изгиба консоли в рамках этих трёх подходов при одинаковом конечном наклоне p_f, особенно для металлов.

Ключевые слова: проблема Эйлера, гипотеза плоских сечений, выгибание, консоль, пластические деформации, диаграмма сжатия, условный предел текучести, критическая выгибающая сила, программирование на Maple, нелинейная оценка, тефлон Al/PTFE, сталь